Synthesis of $La_{1-x}Sr_xAlO_3$ Perovskites by Reverse Strike Co-Precipitation Method and Its Soot Oxidation Activity

Neelapala, Satya Deepika
Department of Chemical Engineering, Manipal Institute of Technology, Manipal Academy of Higher Education, Karnataka, 576104, INDIA

Ashok Yaranal, Naveen
Department of Chemical Engineering, Indian Institute of Technology, Guwahati, Assam, 781039, INDIA

Dasari, Harshini*[+]
Department of Chemical Engineering, Manipal Institute of Technology, Manipal Academy of Higher Education, Karnataka, 576104, INDIA

ABSTRACT: *$La_{1-x}Sr_xAlO_3$ (x=0 to 0.4) perovskite materials were synthesized by reverse strike co-precipitation method and their soot oxidation activity were evaluated. All the catalysts synthesized were characterized using XRD, BET specific surface area, FESEM and XPS techniques. As analyzed by XRD, $La_{1-x}Sr_xAlO_3$ perovskite from x=0 to 0.35 showed the formation of the rhombohedral phase, while for $La_{0.6}Sr_{0.4}AlO_3$ sample the secondary phases SrO, La_2O_3, and Al_2O_3 were also noticed. Sr-doped samples exhibited higher BET specific surface area when compared to pure $LaAlO_3$. FESEM analysis showed that there is a change in morphology upon doping of Sr into $LaAlO_3$ lattice. The O1s spectra observed from XPS analysis showed that the $La_{0.75}Sr_{0.25}AlO_3$ sample contained higher amounts of adsorbed oxygen. La, Sr, and Al existed in +3, +2 and +3 oxidation states respectively in all the synthesized samples as confirmed by XPS. Soot oxidation activity tests showed that $La_{0.75}Sr_{0.25}AlO_3$ exhibited higher catalytic activity relative to other catalysts due to the enhanced amount of reactive adsorbed oxygen species.*

KEYWORDS: *Sr-doped $LaAlO_3$; Reverse strike co-precipitation synthesis; Soot oxidation; Oxygen vacancies.*

INTRODUCTION

Rapid urbanization on one side and higher efficiency, reliability, durability and also lower operational cost on the other side have created a huge demand for a diesel engine. Nonetheless, extensive exhaust treatment is essentially based on the stringent regulations laid on the diesel engine emissions (soot). One of the well-known techniques that mitigate the emission of soot from diesel engines is the use of Catalytic Diesel Particulate Filter (CPDF) which traps the particulate matter and converts the soot by catalytic oxidation to carbon dioxide [1].

* *To whom correspondence should be addressed.*
+ *E-mail: harshini.dasari@manipal.edu*
1021-9986/2019/4/69-77 *9/$/5.09*

In this context, it is worth mentioning that an ideal catalyst must combust soot at a lower temperature with long-lasting activity at the operating conditions of the diesel engine [2]. Perovskite catalysts have been investigated as a predominant group of catalysts ever since their discovery in 1970 because of their high thermal stability, flexibility in achieving a wide range of composition without necessarily changing the structure. Furthermore, there has been extensive literature available regarding the perovskite materials, providing enormous opportunities to work on these materials and to mark them as a suitable candidate for heterogeneous catalytic applications [3]. Though the mechanism of soot oxidation involves multiple steps such as adsorption, spill over, chemisorption, disruption of the complexes, the basic phenomenon is that the active oxygen species are formed on the catalyst's surface from the injected gas phase/sub-surface/ bulk that has to be adsorbed and transferred to the soot [4]. Various works have been reported on the strontium-substituted lanthanum based perovskites in which B-site is mainly of transition metals because of their versatile properties, nevertheless attempts to substitute Sr in $LaAlO_3$ crystal has not been reported yet [5–8]. Our previous work reported that $LaAlO_3$ is rich in lattice oxygen exhibiting high oxygen mobility with good resistance to sintering at elevated temperatures [9]. Based on these reports, it is expected that the incorporation of Sr ions in $LaAlO_3$ may introduce lattice defects and enhance the oxygen vacancies which would in turn, enhance the catalytic soot oxidation by forming active adsorbed oxygen species (O^-, O^{2-}).

The main focus of this work is to develop Strontium doped Lanthanum Aluminum Oxide $La_{1-x}Sr_xAlO_3$ (x=0, 0.2 to 0.4) perovskite materials with the high surface area along with a homogeneous distribution of the dopant cations in the material. It is well known that the method of preparation plays a major role in achieving a homogeneous catalyst [10]. Reverse Strike Co-precipitation (RSC) is used as the synthesis method in this work as it is simple and cost-effective. Uniformity in the samples is easy to achieve through the maintenance of high pH during this precipitation method [11].

EXPERIMENTAL SECTION

Catalyst Preparation

The catalysts were synthesized by Reverse Strike Co-precipitation (RSC) of metal nitrates with ammonium hydroxide solution [12]. The preparation of $LaAlO_3$ in this method is explained in our previous work [9]. Typically, for the preparation of $La_{0.8}Sr_{0.2}AlO_3$, 4.45g of lanthanum (III) nitrate hexahydrate ($La(NO_3)_3.6H_2O$), 0.54g of strontium nitrate ($Sr(NO_3)_2$) and 4.82g of aluminum nitrate nonahydrate ($Al(NO_3)_3$ $.9H_2O$), were dissolved in 100mL of distilled water. This metal nitrate solution was then added dropwise into the base, NH_4OH solution 25% (13.5M) till the pH reached 10 under vigorous stirring. This process resulted in the formation of a brown colored precipitate. This precipitate was then filtered and dried in an oven at 80 °C overnight and calcined at 800 °C for 6h to obtain the final product. Other $La_{1-x}Sr_xAlO_3$ materials were also prepared with the stoichiometric amounts of metal nitrates accordingly.

Characterization

The structural and Phase analysis of the catalysts was done by Rigaku Miniflux 6000, X-ray diffractometer equipped with monochromatized high-intensity Cu Ka radiation (λ=1.54 A°) at a scanning rate of 1°/min in the 2 theta scanning range of 20°-80°. The BET Specific Surface Area was determined by the BET surface area analyzer (Model-SmartSorb 92/93) where all the samples were heated at 200°C to remove the residual moisture. The FESEM images of the prepared materials were obtained on a Hitachi S-1460 using AC voltage of 15 kV. The XPS studies of the as-synthesized catalysts were performed using a Thermo K-5 Alpha XPS instrument equipped with the X-ray source Mg Kα (1253.6 eV) radiation.

Catalytic Activity for Soot Oxidation

The catalytic activity of the synthesized catalysts for soot oxidation was evaluated using Thermogravimetric Analyser TG-DTA instrument (TG/DTA 6300). The measurements were performed with soot-catalyst mixtures (ground in an agate mortar) in 1:4 weight ratio wherein PRINTEX-U was used as model soot under 'tight contact' condition. The experiments were conducted repeatedly for 3 cycles and no noticeable changes in the experimental data were obtained. The catalytic performance in the oxidation of soot was quantified in terms of $T_{1/2}$ °C, the temperature at 50% soot conversion.

RESULTS AND DISCUSSION

XRD analysis

Fig. 1 shows the XRD patterns of $LaAlO_3$ and $La_{1-x}Sr_xAlO_3$ samples, indicating the formation of

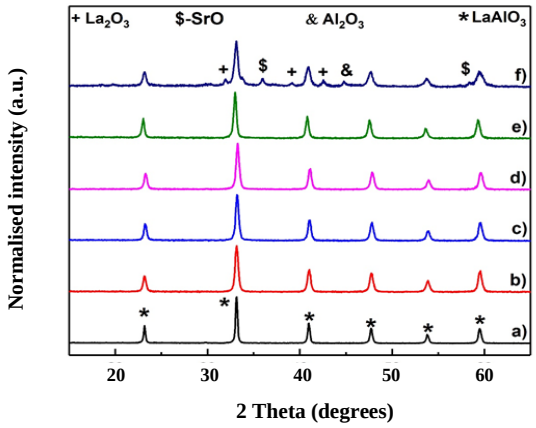

Fig.1: XRD patterns of all the as prepared samples, where a) $LaAlO_3$, b) $La_{0.8}Sr_{0.2}AlO_3$, c) $La_{0.75}Sr_{0.25}AlO_3$, d) $La_{0.7}Sr_{0.3}AlO_3$, e) $La_{0.65}Sr_{0.35}AlO_3$ and f) $La_{0.6}Sr_{0.4}AlO_3$.

Rhombohedral perovskite phase [13] in the samples till x=0.35. There is no evidence of individual oxides phases like La_2O_3, SrO and Al_2O_3 in the diffraction patterns till the Sr dopant level reached 0.35. This confirms the incorporation of Sr^{+2} ions into the $LaAlO_3$ lattice [14–16]. From these XRD patterns, it appears that the rhombohedral structure ($LaAlO_3$) is stable till $La_{0.65}Sr_{0.35}AlO_3$. However, for the $La_{0.6}Sr_{0.4}AlO_3$ perovskite, the formation of respective oxides (although small peaks) along with dominant $LaAlO_3$ phase is noticed. This clearly shows the solubility limit of Sr in $LaAlO_3$ is below 40 (at%) for the samples prepared using this synthesis method.

The lattice constants (a and c) for the rhombohedral structure and the crystallite sizes of the samples, as calculated from XRD analysis are presented in Table 1. It can be seen from the table that the crystal size of the Sr-doped samples have increased which is attributed to the higher ionic radius of Sr^{+2} (1.31 A°) when compared to La^{+3} (1.21 A°) [17]. From the lattice constants determined, though there is an increase in lattice parameter (a), the ratio c/a is maintained the same from Sr^{+2} dopant level (x) = 0.3 representing that the lattice distortions in these samples are similar [18]. It is well known that doping causes lattice distortions that are responsible for the generation of oxygen vacancies and subsequent formation of adsorbed oxygen species [19].

The BET specific surface areas of the undoped $LaAlO_3$ and Sr-doped $La_{1-x}Sr_xAlO_3$ are tabulated in Table 1. Sr-doped samples showed higher values when compared to $LaAlO_3$. This increase in specific surface area for doped compounds states that the $La_{1-x}Sr_xAlO_3$ samples were resistant to thermal sintering compared to pure $LaAlO_3$ [20]. The results depicted that $La_{0.7}Sr_{0.3}AlO_3$ sample showed the highest surface area of 16.2 m^2/g.

FESEM Analysis

Fig. 2 shows the FESEM images of the synthesized compounds. Change in morphology can be noticed with Sr doping into $LaAlO_3$.

From Fig. 2 Sr doped samples $La_{1-x}Sr_xAlO_3$ (x=0.2 to 0.3) exhibited near spherical morphology when compared to pure $LaAlO_3$. These samples also possessed clear boundaries with void spaces specifying that the porous nature has been improved (images b, c, and d). Porous nature increases the contact between the soot and catalysts which will consecutively help in enhancing the soot oxidation activity [21-22]. While for x=0.35 and 0.4 a different morphology has been noticed which might be due to the loss of the perovskite structure and the presence of individual oxides. These results confirm that when the Sr dopant level is $\geq$ 0.3 the perovskite structure of $LaAlO_3$ is not stable. In order to analyze the surface oxygen present in the prepared samples and also to know the oxidation states of La, Sr, and Al in the prepared samples XPS analysis was performed on the materials.

XPS Analysis

XPS is a highly potent tool for determining the surface properties of perovskite materials. It also gives a better understanding of O1s bonding which is essential for determining the catalytic soot oxidation ability of the samples [23]. Fig. 3 represents the O1s spectra of virgin $LaAlO_3$ and Sr-doped compounds. In general, the O1s spectra are split into three sub-bands, the band at lowest binging energy approximately around 528eV corresponds to the lattice oxygen species (O_α), a band at around 530eV relates to surface adsorbed oxygen (O_β), and a band of highest binding energy around 532eV depicts to chemisorbed oxygen (O_γ), due to the presence of water, carbonates or hydroxyls [24]. In the present study, O1s spectra of $LaAlO_3$ exhibited all these three peaks (O_α, O_β, O_γ) [25]. It has been clearly mentioned in the literature that the surface adsorbed oxygen plays a key role in the soot oxidation activity (more the number of oxygen vacancies, higher the oxidation capability) [26].

Table 1: Crystal size, Lattice parameter, and the BET specific surface areas of the prepared catalysts.

Sample	Crystal size (nm)	Lattice Parameter (A°)			Surface Area (m^2/g)
		a	c	(c/a)	
$LaAlO_3$	19.86	3.879	14.145	3.647	6.7
$La_{0.8}Sr_{0.2}AlO_3$	21.79	4.197	13.384	3.189	7.8
$La_{0.75}Sr_{0.25}AlO_3$	22.82	4.201	13.408	3.192	12.9
$La_{0.7}Sr_{0.3}AlO_3$	22.89	4.210	13.407	3.185	16.3
$La_{0.65}Sr_{0.35}AlO_3$	25.66	4.224	13.453	3.185	7.2
$La_{0.6}Sr_{0.4}AlO_3$	20.46	4.219	13.435	3.184	6.1

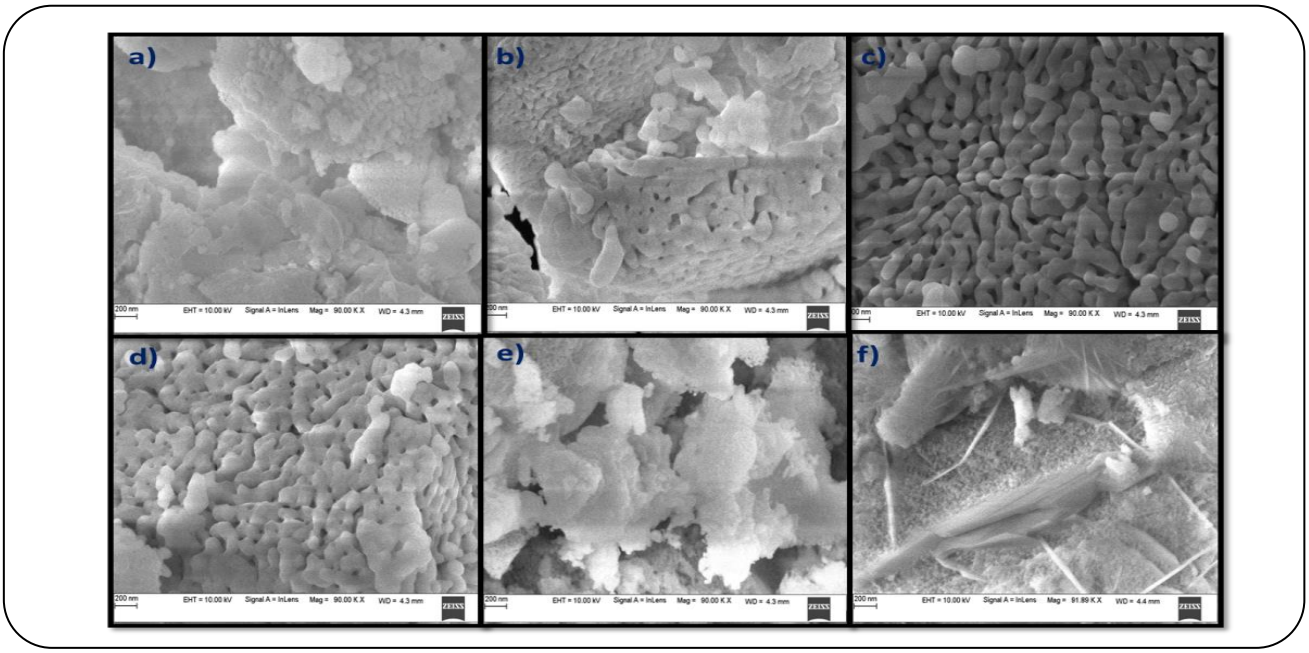

Fig.2: FESEM images of undoped and Sr doped $LaAlO_3$ samples, where a) Undoped $LaAlO_3$, b-f) Sr-doped $La_{1-x}Sr_xAlO_3$ (x=0.2 to 0.4) compounds.

Table 2 gives the % of O_β (the amount of adsorbed oxygen species) and respective binding energies of all the peaks. It depicts an increase in adsorbed oxygen species with an increase in Sr dopant level due to the generation of oxygen vacancies in the perovskite structure resulted from the charge compensation in the A site of the perovskite (as La has +3 oxidation state and Sr is of +2 oxidation state which would lead to charge imbalance).

According to Table 2, the sample with Sr dopant level x=0.25 has a higher percentage of O_β in comparison to other samples. The samples with x=0.2 and 0.25 have the surface adsorbed oxygen peak (O_β) at lower binding energies, while for all the other two samples the peak has shifted to higher binding energies. This shift in the peak will also affect the soot oxidation activity in a way that lower the binding energy, eases the release of adsorbed oxygen species to take part in the oxidation reaction [27]. The binding energy is lowest for $La_{0.75}Sr_{0.25}AlO_3$ sample proving that this sample might show good soot oxidation activity. The similar values of Oβ for the pure $LaAlO_3$ and $La_{0.6}Sr_{0.4}AlO_3$ sample indicates the equal amount of dopant level, though the dopant levels are different in reality. This proves that strontium has not been incorporated properly into the $LaAlO_3$ lattice in this sample[28]. This also coincides with our XRD results.

Table 2: BE and % O_β in the O 1s plot of XPS analysis.

Sample	Binding Energy (eV)			% O_β
	O_α	O_β	O_γ	
1.$LaAlO_3$	530.33	531.52	534.25	43
2.$La_{0.8}Sr_{0.2}AlO_3$	528.34	531.03	533.24	63
3. $La_{0.75}Sr_{0.25}AlO_3$	527.82	530.99	533.14	84
4. $La_{0.7}Sr_{0.3}AlO_3$	529.01	532.84	534.84	56
5. $La_{0.65}Sr_{0.35}AlO_3$	530.77	532.88	535.05	53
6. $La_{0.6}Sr_{0.4}AlO_3$	533.41	534.02	536.73	41

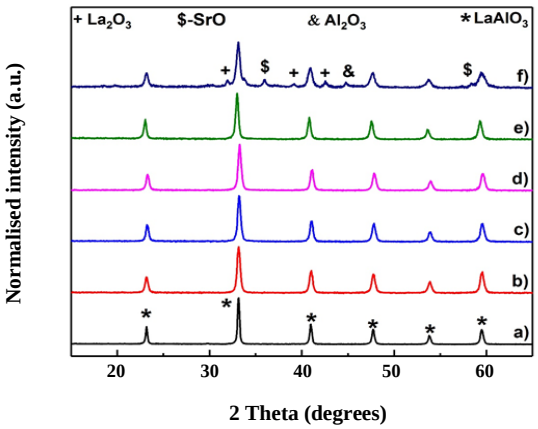

Fig. 3: XPS analysis in the O1s region for all the prepared samples, where a) $LaAlO_3$, b) $La_{0.8}Sr_{0.2}AlO_3$, c) $La_{0.75}Sr_{0.25}AlO_3$, d) $La_{0.7}Sr_{0.3}AlO_3$, e) $La_{0.65}Sr_{0.35}AlO_3$ and f) $La_{0.6}Sr_{0.4}AlO_3$.

The La 3d core-level spectra (Fig.4 (a)) of strontium doped Lanthanum Aluminum Oxide compounds are in good correlation with the literature [29]. The two peaks at 835.2eV and 839.68eV in the La3d spectrum of $LaAlO_3$ corresponds to the characteristic peaks of spin-orbit multiplet $3d_{5/2}$ and the peaks at 852.6eV and 856.4eV relates to the multiplet $3d_{3/2}$. All these peaks determine the oxidation state of La to be +3. These characteristic peaks were observed to be mostly similar over the $La_{1-x}Sr_xAlO_3$ series (x=0.2 to 0.35). Fig.4 (b) represents the core level spectra of Sr 3d with two peaks around 134 eV and 136 eV correspond to $Sr3d_{5/2}$ and $Sr3d_{3/2}$ respectively. This represents the presence of Sr^{+2} in all Sr-doped compounds [30]. The XPS of Al 2p region of the pure $LaAlO_3$ and $La_{1-x}Sr_xAlO_3$ compounds was given in Fig.4 (c). The peak at around 74.9 eV resembles the presence of Al^{+3} in the Sr-doped and stoichiometric lanthanum aluminate ($LaAlO_3$) [31,32].

Catalytic activity in Soot Oxidation

Fig. 5 and Table 3 show the soot oxidation analysis of $LaAlO_3$ and Sr-doped samples. The catalytic activity is determined to be in the order of $La_{0.75}Sr_{0.25}AlO_3$>$La_{0.8}Sr_{0.2}AlO_3$>$La_{0.7}Sr_{0.3}AlO_3$>$La_{0.65}Sr_{0.35}AlO_3$>$LaAlO_3$>$La_{0.6}Sr_{0.4}AlO_3$.

It is interesting to observe that the catalytic soot activity increased with Sr doping (till x=0.25) when compared to $LaAlO_3$ sample. It has been widely mentioned in the literature that phase formation [33], morphology [34] and the presence of surface adsorbed oxygen O_β [35] will enhance the catalytic soot oxidation.

It is obvious that the sample $La_{0.6}Sr_{0.4}AlO_3$ exhibits least catalytic behavior due to formation respective oxides and loss in the perovskite structure as evidenced by XRD and XPS results. This implies that the perovskites structure which is highly active in oxidation reactions is essential for soot oxidation activity. $La_{0.75}Sr_{0.25}AlO_3$ has shown better soot oxidation activity due to the presence of a porous nature (FESEM analysis) and higher amounts of reactive adsorbed oxygen species (from Table 2. XPS of O1s) which resulted from the generation of higher amounts of oxygen vacancies. It is interesting to note here that though $La_{0.7}Sr_{0.3}AlO_3$ possessed a high surface area, the catalytic activity of this sample is lower than $La_{0.75}Sr_{0.25}AlO_3$. This proves that soot oxidation activity is independent of surface area in this work and

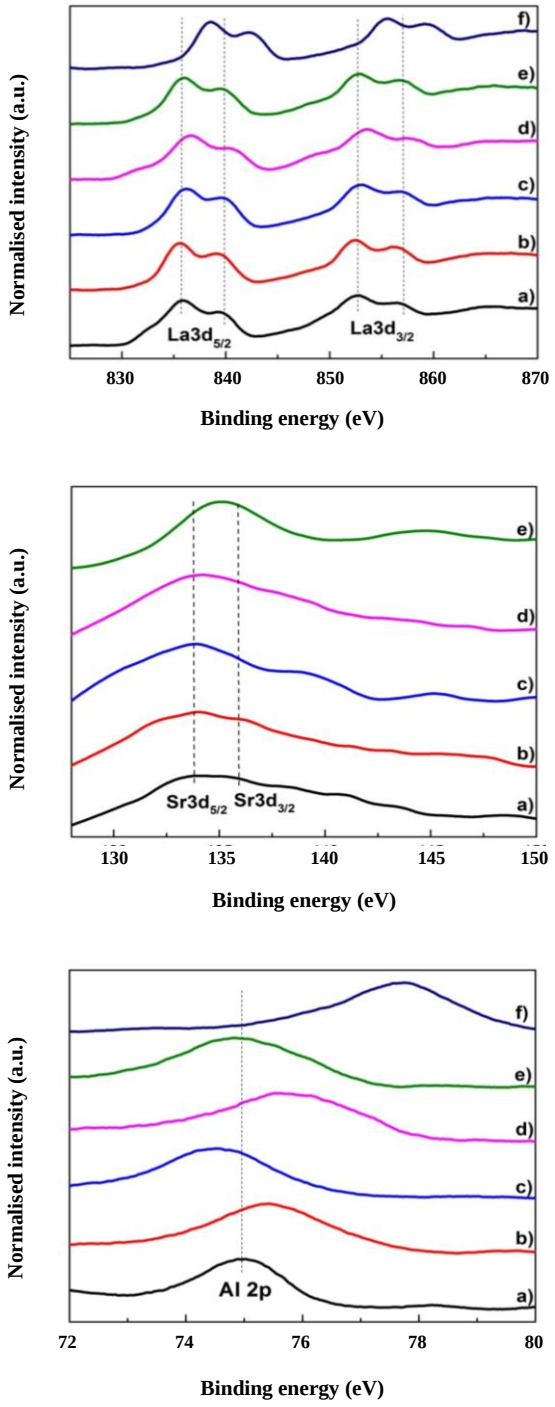

Fig. 4: (a) XPS images in La 3d region of the samples, where a) $LaAlO_3$, b) $La_{0.8}Sr_{0.2}AlO_3$, c) $La_{0.75}Sr_{0.25}AlO_3$, d) $La_{0.7}Sr_{0.3}AlO_3$, e) $La_{0.65}Sr_{0.35}AlO_3$ and f) $La_{0.6}Sr_{0.4}AlO_3$. (b) XPS results by Sr 3d region of the samples, where a) $La_{0.8}Sr_{0.2}AlO_3$, b) $La_{0.75}Sr_{0.25}AlO_3$, c) $La_{0.7}Sr_{0.3}AlO_3$, d) $La_{0.65}Sr_{0.35}AlO_3$ and e) $La_{0.6}Sr_{0.4}AlO_3$. (c) XPS analysis of all the samples with Al 2p region, where a) $LaAlO_3$, b) $La_{0.8}Sr_{0.2}AlO_3$, c) $La_{0.75}Sr_{0.25}AlO_3$, d) $La_{0.7}Sr_{0.3}AlO_3$, e) $La_{0.65}Sr_{0.35}AlO_3$ and f) $La_{0.6}Sr_{0.4}AlO_3$.

is mainly dependent on the presence of O_β which are highly reactive in soot oxidation reactions [36].

Shangguan et al. [37] stated that adsorbed oxygen species play a dynamic role in the soot oxidation process. A similar mechanism can be anticipated in this work also as the soot oxidation activity is determined to be highly influenced by the amount of adsorbed oxygen species.

$$O_{2(gas)} \Leftrightarrow [O_{ads}]$$

$$S_f + O_{ads} \rightarrow SOC$$

$$SOC + O_{ads}/O_{2(gas)} \rightarrow CO/CO_2$$

Where O_{ads} is the adsorbed oxygen species, S_f is a free site on soot and SOC is the Soot Oxygen Complex, which is an intermediate reacts with either $O_{2(gas)}$ or O_{ads} to form soot oxidation products.

CONCLUSIONS

Perovskite series $La_{1-x}Sr_xAlO_3$ (x=0, 0.2 to 0.4) were successfully synthesized by a relatively simple Reverse Strike Co-precipitation (RSC) method and characterized by various analyses such as XRD, BET specific surface area, FESEM and XPS analysis. The soot oxidation activity of all the samples was evaluated with the help of Thermogravimetric analysis. XRD patterns concluded the formation of Rhombohedral phase structure for $La_{1-x}Sr_xAlO_3$ perovskites till x=0.3 and respective oxides were seen when x=0.4, indicating that the solubility limit of Sr in $LaAlO_3$ lattice is below 40 (at%). Sr-doped samples (till x=0.35) exhibited a higher specific surface area when compared to pure $LaAlO_3$. The doped samples $La_{1-x}Sr_xAlO_3$ appeared spherical and porous with clear boundaries when compared to pure $LaAlO_3$ as evidenced by FESEM analysis. XPS investigations confirmed the existence of La, Sr and Al in +3, +2 and +3 oxidation states respectively. The amount of adsorbed oxygen species was found to be increased with Sr doping till x=0.25. Among all the samples, $La_{0.75}Sr_{0.25}AlO_3$ exhibited a higher amount of adsorbed oxygen species probably due to the generation of more oxygen vacancies. Thus, from this study it can be concluded that reactive adsorbed oxygen species played a key role in enhancing the soot oxidation activity.

Table 3: $T_{1/2}$ temperatures for the soot oxidation.

S.No.	Sample	$T_{1/2}$ (°C)
1	$LaAlO_3$	450
2	$La_{0.8}Sr_{0.2}AlO_3$	428
3	$La_{0.75}Sr_{0.25}AlO_3$	410
4	$La_{0.7}Sr_{0.3}AlO_3$	434
5	$La_{0.65}Sr_{0.35}AlO_3$	444
6	$La_{0.6}Sr_{0.4}AlO_3$	500

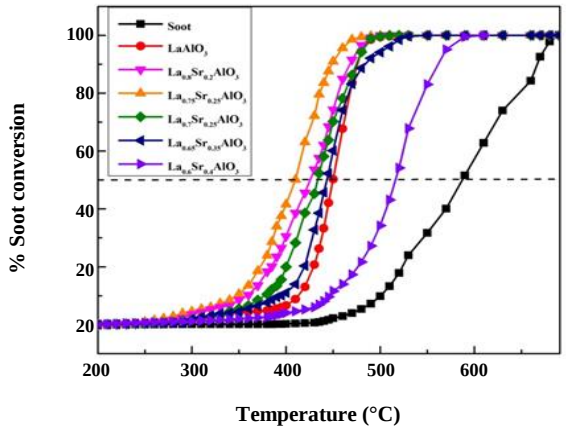

Fig. 5: Soot oxidation results of the undoped and Sr doped $LaAlO_3$ samples.

Acknowledgments

This project was supported by Korea Institute of Science and Technology, the Republic of Korea under KIST Alumni project with the project code 2Z04820-16- 092.

Received : Dec. 13, 2017 ; Accepted : Jun. 18, 2018

REFERENCES

[1] Royer S., Duprez D., Can F., Courtois X., Batiot-Dupeyrat C., S. Laassiri, H. Alamdari, Perovskites as Substitutes of Noble Metals for Heterogeneous Catalysis: Dream or Reality, *Chem. Rev.*, **114**: 10292-10368 (2014).

[2] Keav S., Matam S., Ferri D., Weidenkaff A., Structured Perovskite-Based Catalysts and Their Application as Three-Way Catalytic Converters—A Review, *Catalysts*, **4**: 226–255 (2014)

[3] Tanaka H., Misono M., Advances in Designing Perovskite Catalysts, *Curr. Opin. Solid State Mater. Sci.*, **5**: 381–387 (2001).

[4] Leistner K., Nicolle A., Da Costa P., Impact of the Catalyst/Soot Ratio on Diesel Soot Oxidation Pathways, *Energy and Fuel*, **26**: 6091–6097 (2012).

[5] Liu X., Su W., Lu Z., Liu J., Pei L., Liu W., He L., Mixed Valence State and Electrical Conductivity of $La_{1-x}Sr_xCrO_3$, *J. Alloys Compd.*, **305**: 21–23 (2000).

[6] Tabata K., Kohiki S., Catalytic Properties and Surface States of $La_{1-x}(Th, Sr)_xCoO_3$, *J. Mater. Sci.*, **22**: 3781–3783 (1987).

[7] Deng J., Zhang L., Dai H., He H., Au C.T., Strontium-Doped Lanthanum Cobaltite and Manganite: Highly Active Catalysts for Toluene Complete Oxidation, *Ind. Eng. Chem. Res.*, **47**: 8175–8183 (2008).

[8] Kim C.H., Qi G., Dahlberg K., Li W., Strontium-Doped Perovskites Rival Platinum Catalysts for Treating NO_x in Simulated Diesel Exhaust, *Science*, **327**:1624–1627 (2010).

[9] Harshini D., Yoon C.W., Han J., Yoon S.P., Nam S.W., Lim T.-H., Catalytic Steam Reforming of Propane over $Ni/LaAlO_3$ Catalysts: Influence of Preparation Methods and OSC on Activity and Stability, *Catal. Letters*, **142**: 205–212 (2012).

[10] Piumetti M., Russo N., Miceli P., Bensaid S., Russo N., Fino D., Bensaid S., Russo N., Fino D., Study on the CO Oxidation over Ceria-Based Nanocatalysts, *Nanoscale Res. Lett.*, **11**: 165- (2016).

[11] Zhang K., Liu H., Wu Y., Hu W., Co-precipitation Synthesis and Luminescence Behavior of Ce-Doped Yttrium Aluminum Garnet (YAG : Ce) Phosphor : The Effect of Precipitant, *J. Alloys Compd.*, **453**: 265–270 (2008).

[12] Doggali P., Subrt Æ.S.B.Æ.J., Haneda T.M.Æ.H., Labhsetwar Æ.N., Low Cost Ceria Promoted Perovskite Type Catalysts for Diesel Soot Oxidation, *Catal. Lett.*, **131**:137–143. (2008).

[13] Azough F., Wang W., Freer R., The Crystal Structure of $LaAlO_3$ Stabilized $LaTiO_3$ Ceramics: An HRTEM Investigation, *J. Am. Ceram. Soc.*, **92**:2093–2098 (2009).

[14] Gerber L.C., Moser N., Luechinger N.A., Stark W.J., Grass R.N., Supporting Information for : Phosphate Starvation as an Antimicrobial Strategy : The Controllable Toxicity of Lanthanum Oxide Nanoparticles Content : A) X-Ray Diffraction Analysis, *RSC*., 1–5 (2012).

[15] Zhang S., Pang R., Jiang L., Li D., Jia Y., Li H., Sun W., Li C., Highly Active MnO_x–CeO_2 Catalyst for Diesel Soot Combustion, *RSC Advances*, **7**: 3233-3239 (2015).

[16] Guiti F., Olga C., An Efficient and Recyclable 3D Printed α-Al_2O_3 Catalyst for the Multicomponent Assembly of Bioactive Heterocycles, *Applied Catal. A, Gen*., (2016). doi:10.1016/j.apcata.2016.11.031.

[17] Prasad D.H., Park S.Y., Oh E., Ji H., Kim H., Yoon K., Son J., Lee J., Synthesis of Nano-Crystalline $La_{1-x}Sr_xCoO_3$ Perovskite Oxides by EDTA – Citrate Complexing Process and its Catalytic Activity for Soot Oxidation, *Applied Catalysis A : General*, **448** : 100–106 (2012).

[18] Lei S., Fan H., Chen W., Effects of CaO-B_2O_3 Glass Addition on the Low-Temperature Sintering and Cation Ordering in $Sr_xLa_{(1-x)}Ti_xAl_{(1-x)}O_3$ Ceramics, *J. Alloys Compd*., **632**: 78–86. (2015)

[19] Gupta A., Waghmare U.V., Hegde M.S., Correlation of Oxygen Storage Capacity and Structural Distortion in from First Principles Calculation, *Chem.Mater*., **22**: 5184–5198 (2010).

[20] Katta L., Sudarsanam P., Thrimurthulu G., Reddy B.M., Doped Nanosized Ceria Solid Solutions for Low Temperature Soot Oxidation: Zirconium Versus Lanthanum Promoters, *Appl. Catal. B Environ.*, **101**: 101–108 (2010).

[21] Shao W., Wang Z., Zhang X., Wang L., Promotion Effects of Cesium on Perovskite Oxides for Catalytic Soot Combustion, *Catal. Letters*, **146**: 1397–1407 (2016).

[22] Liu L.Z., Li T.H., Wu X.L., Shen J.C., Chu P.K., Identification of Ooxygen Vacancy Types from Raman Spectra of SnO_2 Nanocrystals, *J. Raman Spectrosc.*, **43**(10): 1423-1426 (2012).

[23] Piumetti M., Bensaid S., Russo N., Fino D., Investigations into Nanostructured Ceria-Zirconia Catalysts for Soot Combustion, *Appl. Catal. B Environ.*, **180**: 271–282 (2016).

[24] Fang C., Zhang D., Shi L., Gao R., Li H., Ye L., Zhang J., Highly Dispersed CeO_2 on Carbon Nanotubes for Selective Catalytic Reduction of NO with NH_3, *Catalysis Science & Technology*, **3**: 803–811 (2013).

[25] Pawlak D.A., Ito M., Oku M., Shimamura K., Fukuda T., Interpretation of XPS O (1s) in Mixed Oxides Proved on Mixed Perovskite Crystals, *J. Phys. Chem. B.*, **106**: 504–507(2002).

[26] Xin Z., Qiuhua Y., Jinjin C.U.I., XPS Study of Surface Absorbed Oxygen of ABO_3 Mixed Oxides, *Journal of Rare Earths*, **26**: 511–514 (2008).

[27] Huang H., Liu J., Sun P., Ye S., Liu B., Effects of Mn-Doped Ceria Oxygen-Storage Material on Oxidation Activity of Diesel Soot, *RSC Adv*., **7**: 7406–7412 (2017).

[28] Lin F., Delmelle R., Vinodkumar T., Reddy B.M., Wokaun A., Alxneit I., Correlation between the Structural Characteristics, Oxygen Storage Capacities and Catalytic Activities of Dual-Phase Zn-Modified Ceria Nanocrystals, *Catal. Sci. Technol*,. **5**: 3556–3567 (2015).

[29] Sunding M.F., Hadidi K., Diplas S., Løvvik O.M., Norby T.E., Gunnæs A.E., XPS Characterisation of in Situ Treated Lanthanum Oxide and Hydroxide Using Tailored Charge Referencing and Peak Fitting Procedures, *J. Electron Spectros. Relat. Phenomena.* **184**: 399-400 (2011).

[30] Wu Q.-H., Liu M., Jaegermann W., X-Ray Photoelectron Spectroscopy of $La_{0.5}Sr_{0.5}MnO_3$, *Mater. Lett.*, **59**: 1980–1983 (2005)

[31] Miotti L., Driemeier C., Tatsch F., Radtke C., Edon V., Hugon M.C., Voldoire O., Agius B., Baumvol I.J.R., Atomic Transport in $LaAlO_3$ Films on Si Induced by Thermal Annealing, *Electrochem. Solid-State Lett.*, **9**: 49–52 (2006).

[32] Koushik D., Verhees W., Kuang Y., Veenstra S., Zhang D., Verheijen M.A., Creatore M., Schropp R.E.I.E.I., High-Efficiency Humidity-Stable Planar Perovskite Solar Cells Based on Atomic Layer Architecture,*Energy & Environmental Science*, 0–31 (2016). doi:10.1039/C6EE02687G.

[33] Andana T., Piumetti M., Bensaid S., Russo N., Fino D., Pirone R., CO and Soot Oxidation over Ce-Zr-Pr Oxide Catalysts, *Nanoscale Res. Lett.*, **11**: 278 (2016). doi:10.1186/s11671-016-1494-6.

[34] Miceli P., Bensaid S., Russo N., Fino D., Effect of the Morphological and Surface Properties of CeO_2-Based Catalysts on the Soot Oxidation Activity, *Chem. Eng. J.*, **278**:190–198 (2015).

[35] Imai H., Mechanistic Aspects of Oxidative Coupling of Methane, *J. Chem. SOC., Faraday Trans. 1*, **84**: 923–929 (1988).

[36] Liu F., He H., Ding Y., Zhang C., Effect of Manganese Substitution on the Structure and Activity of Iron Titanate Catalyst for the Selective Catalytic Reduction of NO with NH_3, *Applied Catalysis B. Environmental*, **93**: 194–204 (2009).

[37] Shangguan W.F., Teraoka Y., Kagawa S., Kinetics of Soot-O_2, Soot-NO and Soot-O_2-NO Reactions over Spinel-Type $CuFe_2O_4$ Catalyst, *Applied Catalysis B. Environmental*,**12**: 237–247 (1997).